Supplement of

Top-down and bottom-up estimates of anthropogenic methyl bromide emissions from eastern China

Haklim Choi[1], Mi-Kyung Park[1], Paul J. Fraser[2], Hyeri Park[3], Sohyeon Geum[3], Jens Mühle[4], Jooil Kim[4], Ian Porter[5], Peter K. Salameh[4], Christina M. Harth[4], Bronwyn L. Dunse[2], Paul B. Krummel[2], Ray F. Weiss[4], Simon O'Doherty[6], Dickon Young[6], and Sunyoung Park[1,3]

[1]Kyungpook Institute of Oceanography, Kyungpook National University, Daegu 41566, Republic of Korea
[2]Climate Science Centre, Commonwealth Scientific and Industrial Research Organisation (CSIRO) Oceans and Atmosphere, Aspendale, Victoria 3195, Australia
[3]Department of Oceanography, Kyungpook National University, Daegu 41566, Republic of Korea
[4]Scripps Institution of Oceanography, University of California San Diego, La Jolla, CA 92093, USA
[5]School of Life Sciences, La Trobe University, Bundoora, Victoria 3086, Australia
[6]Atmospheric Chemistry Research Group, University of Bristol, Bristol BS8 1TS, UK

Correspondence to: Sunyoung Park (sparky@knu.ac.kr)

Potential source regions

The regional distribution of potential CH_3Br sources in East Asia was derived by applying a statistical analysis to the air mass trajectories that correspond to the enhancements of CH_3Br above baseline at Gosan during 2008-2019. Among the various trajectory-based statistical approaches, we applied a trajectory statistics method based on Seibert et al. (1994) to identify the potential sources of atmospheric pollutants (Reimann et al., 2004; Li et al., 2014). This method assumes that the concentration enhancement above baseline at the observation site is proportional to the average concentration of each grid cell through which the air mass has passed and the residence time that the air mass spends in each grid cell. Therefore, the residence-time-weighted mean concentration $\overline{C_{mn}}$ of a target compound in each grid on the domain can be calculated as follows:

$$\overline{C_{mn}} = \frac{\sum_i^M (\tau_{mni} c_i)}{\sum_i^M \tau_{mni}}, \qquad \text{S(1)}$$

where m,n is a potential source region of CH_3Br - *m,n* are indices of a horizontal grid cell, *i* is the index of the trajectory and *M* is the total number of trajectories, C_i is the enhanced concentration of CH_3Br above baseline and τ_{mni} is the residence time that trajectory *i* spent over the grid cell *m,n* within the atmospheric boundary layer. The calculation of the residence time over each grid was accomplished using the method of Poirot and Wishinski (1986), which assumes that an air parcel travels linearly between two points at constant speed.

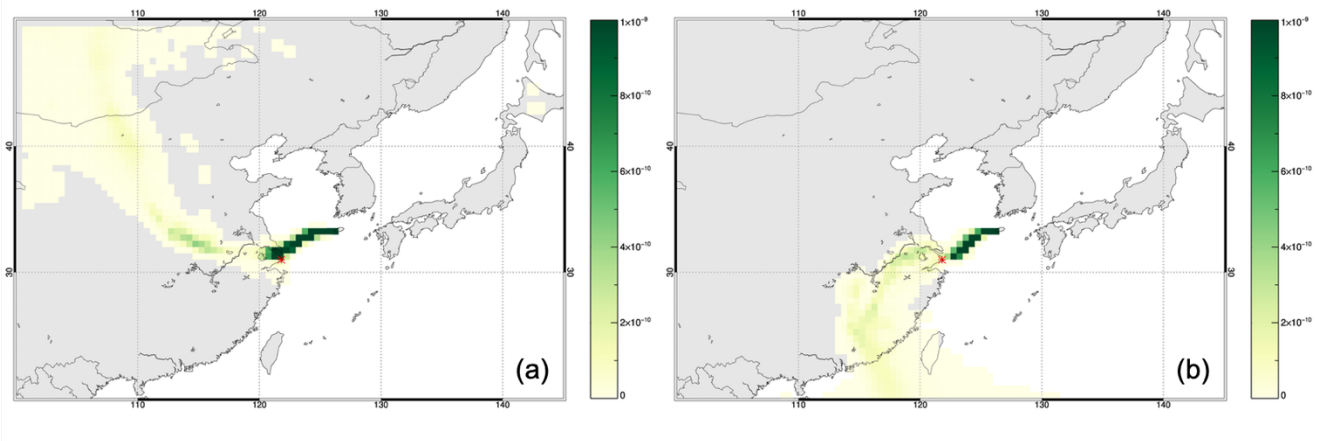

Figure S1: Spatial distributions of residence time simulated from the FLEXible PARTicle dispersion model (FLEXPART) (a) 12 UTC on 4 May 2016 and (b) 05 UTC on 4 January 2015. The Lagrangian back trajectories were computed for a large number of notional particles (n=50,000). The observed concentration of CH_3Br were (a) 41.2 ppt and (b) 25.3 ppt, respectively. The location of the port of Shanghai is marked with a red asterisk.

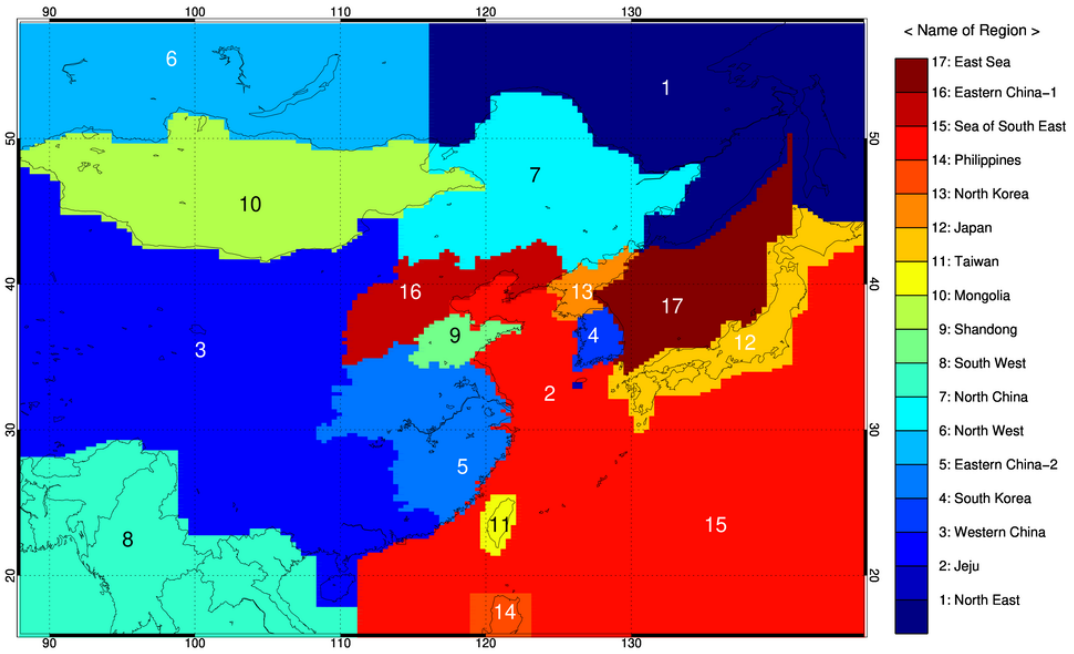

Figure S2a: The division of East Asia into 17 named potential source regions.

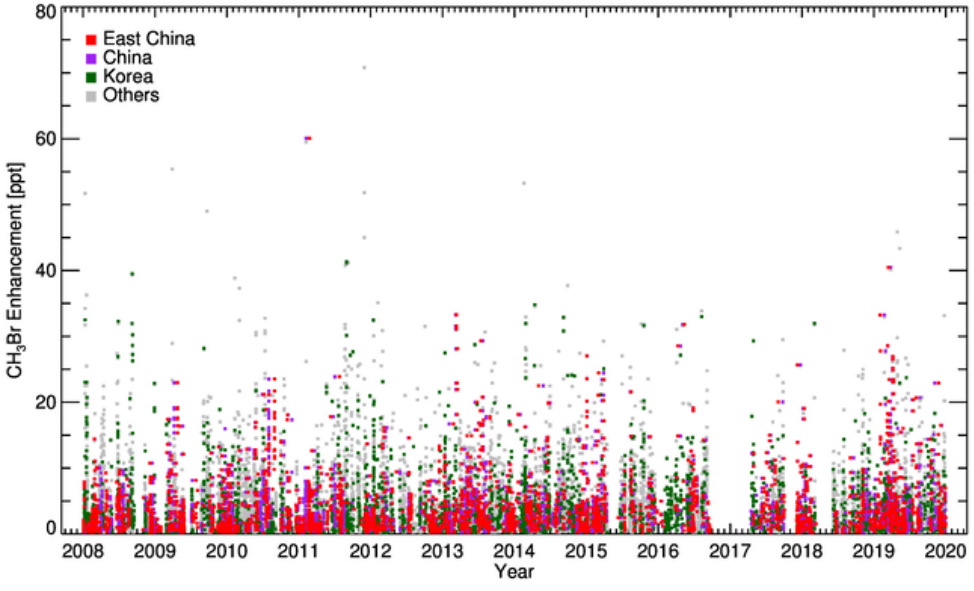

Figure S2b: The time series of enhanced concentrations of CH_3Br for 2008-2019; the aggregated air-mass regional origins are shown as red (eastern China), purple (China), green (Korea), and others (grey), respectively.

Fig. S2a shows the 17-potential source regions for East Asia. The regional origin of an air-mass that inflows to Gosan is classified from the backward trajectory analysis using HYSPLIT. In this study, the aggregated source regions were designated as China (3, 5, 7, 9 and 16), eastern China (5, 9 and 16), Korea (2, 4 and 13) and the remining regions were classified as others. Eastern China-1 consists of Beijing, Liaoning, Tianjin, Hebei and Shanxi provinces, while eastern China-2 consists of Henan, Hubei, Anhui, Jiangsu, Shanghai, Jiangxi, Zhejiang and Fujian provinces.

Fig. S2b is the time series of CH_3Br enhancements (pollution – baseline) for the same period as shown in Fig. 2 of the main manuscript; the regional origin of each air mass is indicated by colour with regards to the 17 regions (Fig S2a), aggregated to east China, China, Korea and others.

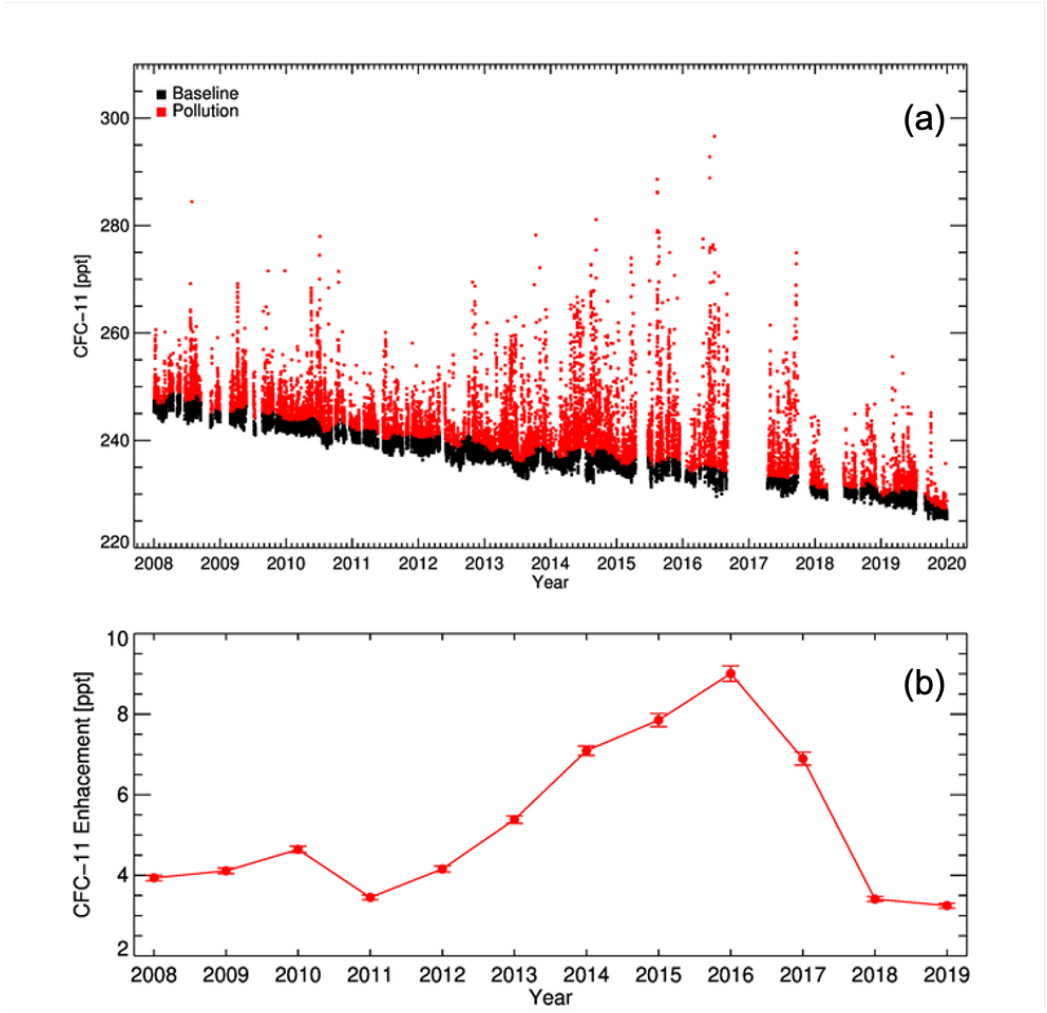

Figure S3: (a) Concentration of CFC-11 in the atmosphere observed at Gosan in the period 2008–2019 (Park et al., 2021); the baseline data are shown in black determined by a statistical filtering method (O'Doherty et al., 2001); the polluted data (elevated above the baseline data) are shown in red. (b) The time series for the annual average of enhancement of CFC-11 above baseline; the error bars denote the standard error of the mean (there are typically 175 data points per annual mean).

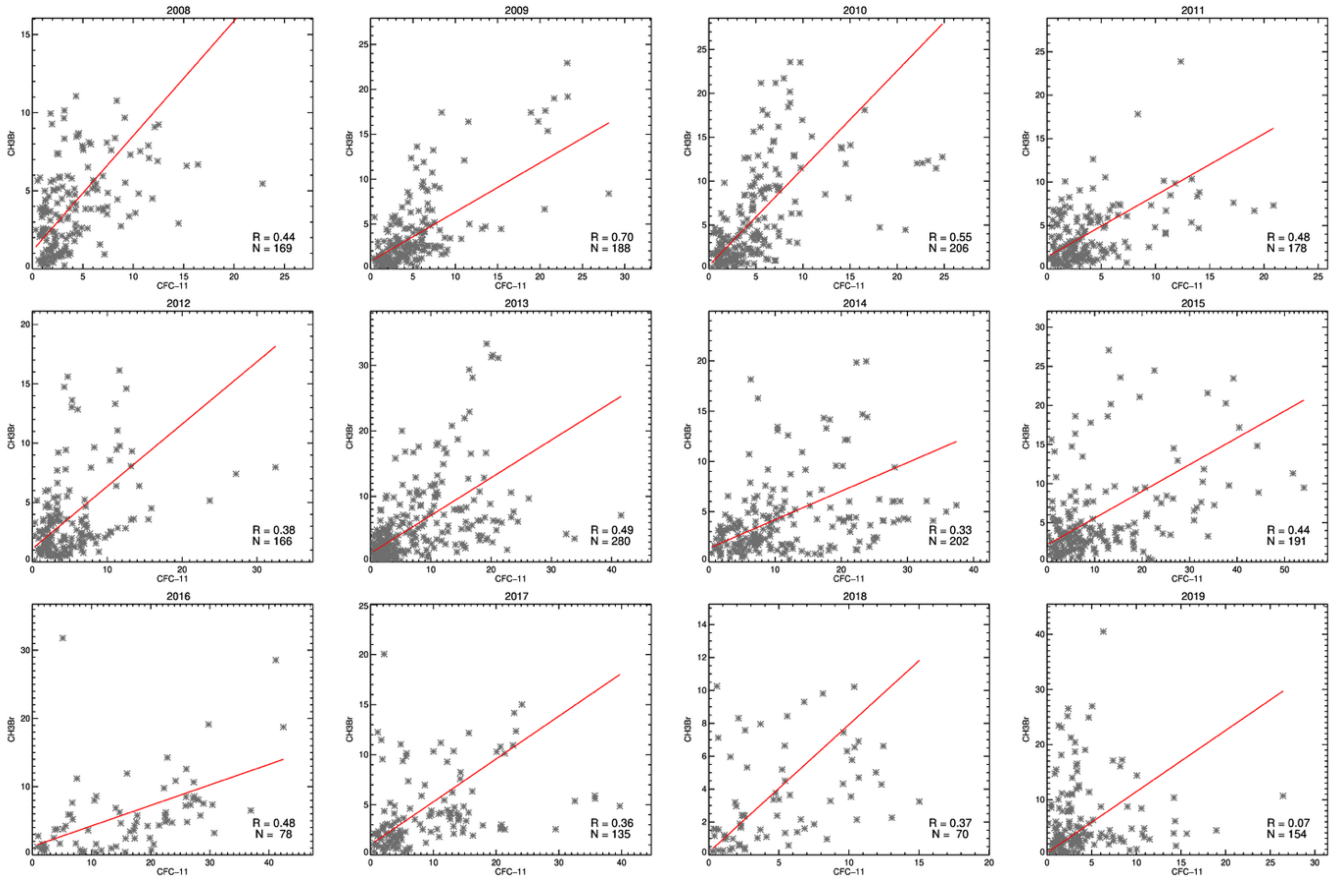

Figure S4: The annual correlation between the enhancement of CH_3Br and CFC-11 above baseline measured at Gosan from 2008 to 2019. The linear trend line was derived by the Deming regression method (see text).

Figure S4 shows the xy plot of the annual enhancements of CH_3Br and CFC-11 above baseline. The linear correlations between the two pollutants were derived from the weighted Deming regression method suggested (Wu and Yu, 2018), showing significant correlations each year between the two pollutants. Note that the Pearson correlation coefficient in 2019 was very low ($R < 0.1$) because of a tendency for the data in 2019 to bifurcate due to the occurrence of some high concentration cases from different source regions to the source regions for the majority of the low enhancement concentrations. For 2019, we adopted the slope and uncertainty of the regression line in 2010, which were used to estimate the emissions of CH_3Br for 2019 by using the ISC method.

Table S1: Annual slopes term and their uncertainties between CH_3Br and CFC-11 as shown in Figure S4.

Year	CH_3Br *vs.* CFC-11	
	Slope	Uncertainty of slope
2008	0.74	0.18
2009	0.55	0.09
2010	1.10	0.12
2011	0.71	0.12
2012	0.53	0.25
2013	0.58	0.07
2014	0.28	0.04
2015	0.34	0.13
2016	0.30	0.07
2017	0.43	0.09
2018	0.77	0.11
2019*	1.10	0.12

* Note: slope and uncertainty for 2019 used 2010 values.

Table S2: Global CH_3Br emissions for QPS and non-QPS from 2008 to 2019.

Year	UNEP reported (Gg yr^{-1})	
	QPS	non-QPS
2008	7.38	6.85
2009	7.67	5.74
2010	9.20	4.95
2011	8.15	3.14
2012	7.44	2.27
2013	8.25	1.56
2014	9.34	0.69
2015	6.87	0.35
2016	7.01	0.61
2017	8.32	0.23
2018	8.97	0.00
2019*	7.53	0.01

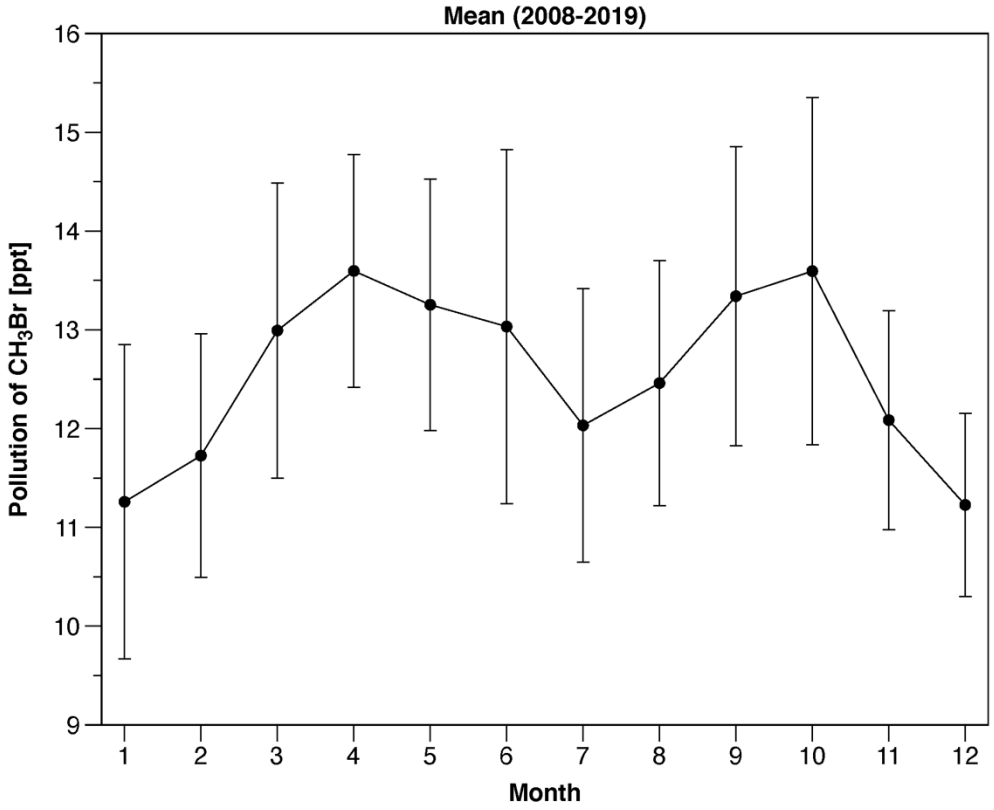

Figure S5: Monthly mean of polluted concentrations of CH_3Br at Gosan from 2008 to 2019.

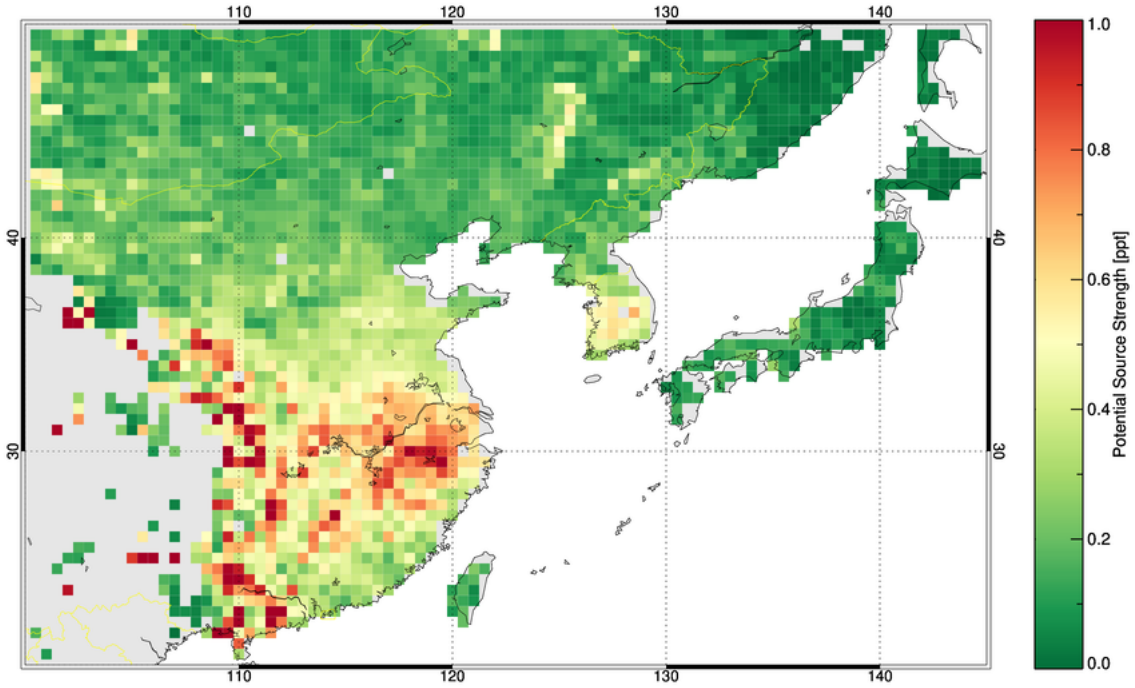

90

Figure S6: Potential source regions derived from back-trajectory analyses of SO_2F_2 pollution data at Gosan from 2008 to 2019.

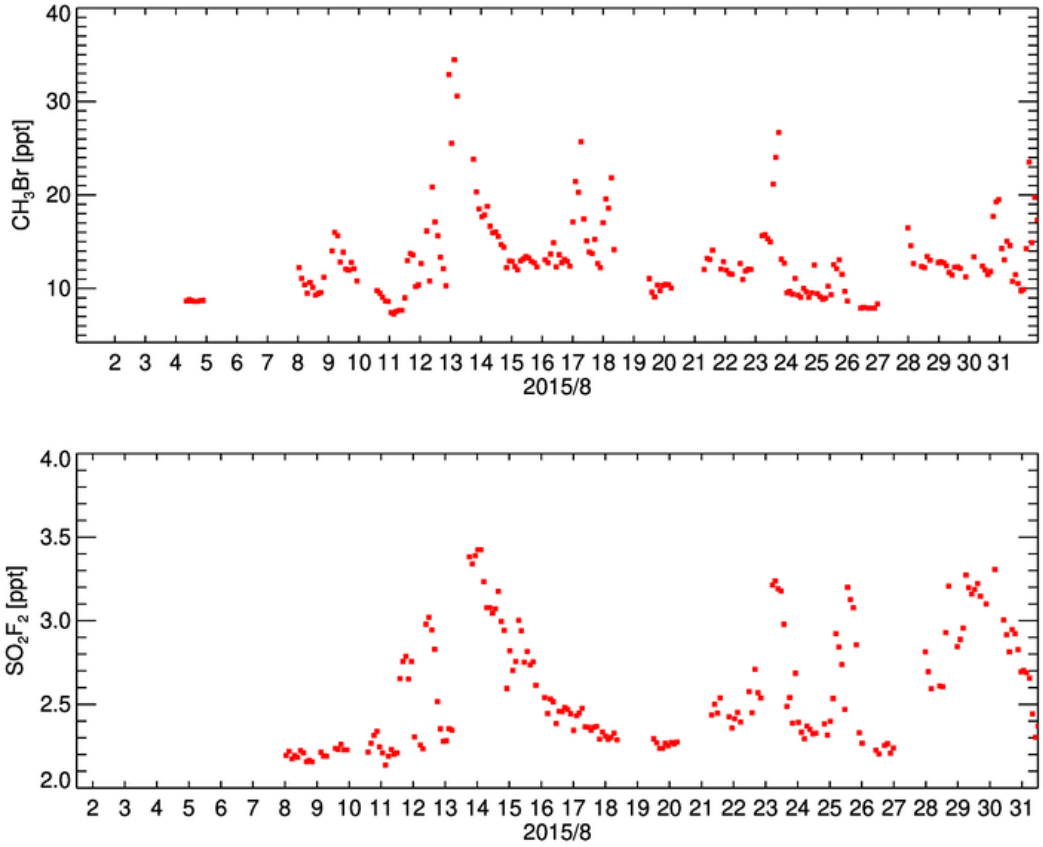

Figure S7: Observed concentrations of CH_3Br and SO_2F_2 at Gosan during August 2015; note the correlated and non-correlated pollution events.

95

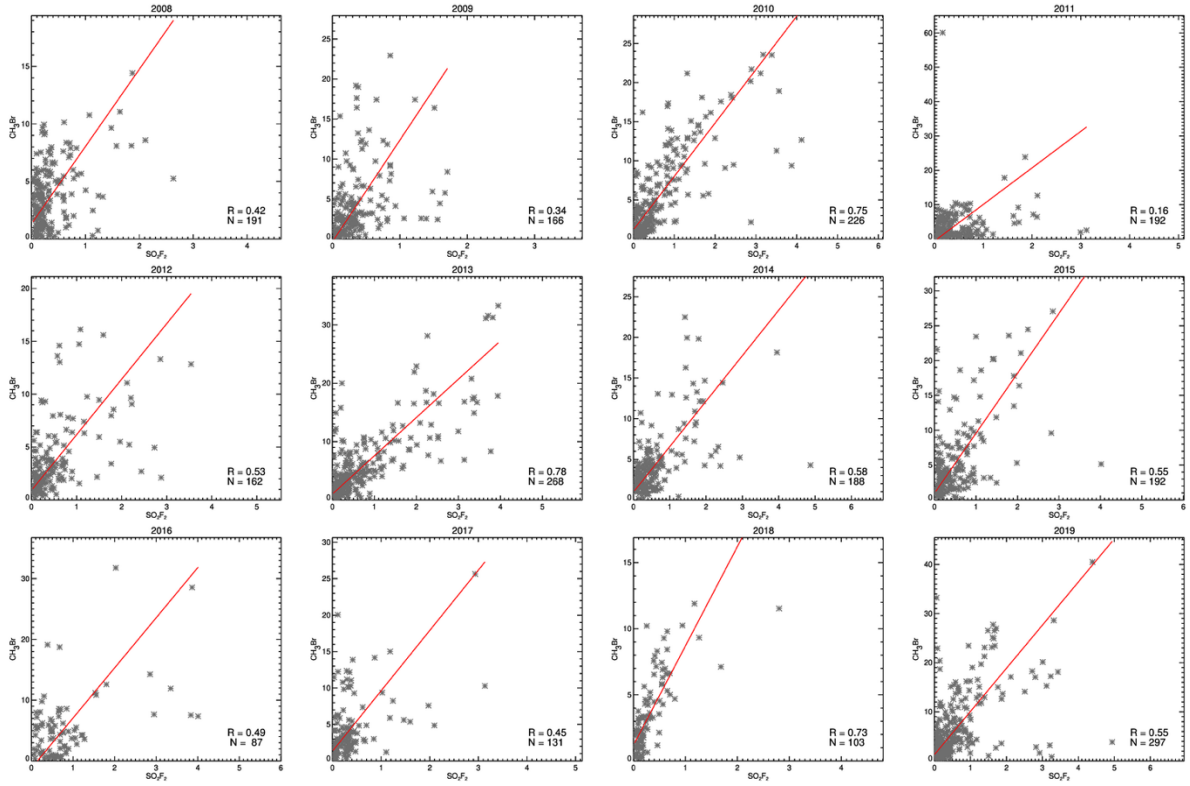

Figure S8: Same as Figure S4, but for CH_3Br and SO_2F_2.

Table S3: Same as Table S1, but for CH_3Br and SO_2F_2 as shown in Figure S8.

Year	CH_3Br *vs.* SO_2F_2	
	Slope	Uncertainty of slope
2008	6.71	1.27
2009	12.70	3.39
2010	6.83	0.43
2011	10.65	6.26
2012	5.25	0.75
2013	6.56	0.34
2014	5.60	0.65
2015	8.60	1.07
2016	8.25	1.81
2017	8.28	1.71
2018	7.51	0.74
2019	8.78	0.88

SI. References

Li, S., Kim, J., Park, S., Kim, S. K., Park, M. K., Mühle, J., Lee, G., Lee, M., Jo, C. O. and Kim, K. R.: Source identification and apportionment of halogenated compounds observed at a remote site in East Asia, Environ. Sci. Technol., doi:10.1021/es402776w, 2014.

O'Doherty, S., Simmonds, P. G., Cunnold, D. M., Wang, H. J., Sturrock, G. A., Fraser, P. J., Ryall, D., Derwent, R. G., Weiss, R. F., Salameh, P., Miller, B. R. and Prinn, R. G.: In situ chloroform measurements at Advanced Global Atmospheric Gases Experiment atmospheric research stations from 1994 to 1998, J. Geophys. Res. Atmos., doi:10.1029/2000JD900792, 2001.

Park, S., Western, L. M., Saito, T., Redington, A. L., Henne, S., Fang, X., Prinn, R. G., Manning, A. J., Montzka, S. A., Fraser, P. J., Ganesan, A. L., Harth, C. M., Kim, J., Krummel, P. B., Liang, Q., Mühle, J., O'Doherty, S., Park, H., Park, M.-K., Reimann, S., Salameh, P. K., Weiss, R. F. and Rigby, M.: A decline in emissions of CFC-11 and related chemicals from eastern China, Nature, doi:10.1038/s41586-021-03277-w, 2021.

Poirot, R. L. and Wishinski, P. R.: Visibility, sulfate and air mass history associated with the summertime aerosol in northern Vermont, Atmos. Environ., doi:10.1016/0004-6981(86)90018-1, 1986.

Reimann, S., Schaub, D., Stemmler, K., Folini, D., Hill, M., Hofer, P., Buchmann, B., Simmonds, P. G., Greally, B. R. and O'Doherty, S.: Halogenated greenhouse gases at the Swiss High Alpine Site of Jungfraujoch (3580 m asl): Continuous measurements and their use for regional European source allocation, J. Geophys. Res. Atmos., doi:10.1029/2003jd003923, 2004.

Seibert, P., Kromp-Kolb, H., Baltensperger, U., Jost, D. T. and Schwikowski, M.: Trajectory Analysis of High-Alpine Air Pollution Data, in Air Pollution Modeling and Its Application X., 1994.

Wu, C. and Zhen Yu, J.: Evaluation of linear regression techniques for atmospheric applications: The importance of appropriate weighting, Atmos. Meas. Tech., doi:10.5194/amt-11-1233-2018, 2018.